Tellus (2007), 59B, 57–65
Printed in Singapore. All rights reserved

TELLUS

Evidence for inertial droplet clustering in weakly turbulent clouds

By KATRIN LEHMANN[1]*, HOLGER SIEBERT[1], MANFRED WENDISCH[1] and RAYMOND A. SHAW[2], [1]*Leibniz-Institute for Tropospheric Research, Permoser Str. 15, 04318 Leipzig, Germany;* [2]*Department of Physics, Michigan Technological University, 1400 Townsend Drive, Houghton, MI 49931-1295, USA*

(Manuscript received 20 March 2006; in final form 22 September 2006)

ABSTRACT

Simultaneous observations of cloud droplet spatial statistics, cloud droplet size distribution and cloud turbulence were made during several cloud passages, including cumulus clouds and a stratus cloud. They provide evidence that inertial droplet clustering occurs even in weakly turbulent clouds. The measurements were made from the Airborne Cloud Turbulence Observation System suspended from a tethered balloon. For a profile through a stratus cloud with gradually changing droplet Stokes number, droplet clustering, quantified by the pair correlation function, is observed to be positively correlated with the droplet Stokes number. This implies that the droplet collision rate, which is relevant to drizzle formation via droplet coalescence, depends not only on the droplet size distribution, but also on the cloud turbulence. For cumulus clouds, the relation between droplet clustering and Stokes number seems more complicated. Stokes number is determined by measuring droplet size and local energy dissipation rate, the latter requiring high-resolution air velocity measurements not possible on fast-flying aircraft.

1. Introduction

The possible influence of turbulence on cloud microphysical properties has been recognized for many years (Saffman and Turner, 1956; Pruppacher and Klett, 1997, sec. 14.5.2). In particular, the interactions between a turbulent velocity field and cloud droplets have come into focus recently. Due to their inertia, cloud droplets do not exactly follow the velocity field and thus tend to converge in regions of high strain and diverge in areas of high vorticity (Maxey, 1987; Sundaram and Collins, 1997). It has been hypothesized that the local clustering of cloud droplets, also referred to as preferential concentration, can enhance both the condensational growth of droplets and the growth of droplets by collision and coalescence (Falkovich et al., 2002; Shaw, 2003; Franklin et al., 2005). For example, the mean collision rate increases as a result of positive fluctuations in the local droplet number concentration due to inertial droplet clustering. Theory suggests that droplets interact most strongly with the surrounding turbulence when the particle Stokes number, defined as

$$St = \frac{\tau_p}{\tau_f} = \frac{\rho_w\, d^2\, \varepsilon^{1/2}}{18\, \rho_a\, \nu^{3/2}}, \tag{1}$$

is close to one (Wang and Maxey, 1993). Here, τ_p is the particle response time, τ_f the typical fluid timescale, ρ_w and ρ_a represent the densities of water and air, d the droplet diameter, $\nu = 1.5 \times 10^{-5}\ \mathrm{m^2\ s^{-1}}$ the kinematic viscosity of air and ε the turbulent kinetic energy dissipation rate ($10^{-2}\ \mathrm{m^2\ s^{-3}}$ is a typical value in cumulus clouds). Because inertial clustering is associated with vorticity, and the power spectrum of vorticity peaks at dissipation scales (Tennekes and Lumley, 1972), the Kolmogorov timescale is the relevant fluid timescale, such that $\tau_f = (\nu/\varepsilon)^{1/2}$. If the Stokes number vanishes, droplets do not posses inertia and exactly follow the streamlines of the velocity field, thus acting as tracers of the flow. At the other extreme, for $St \gg 1$, droplets have such large inertia that they do not respond significantly to fluid accelerations on the timescale of those accelerations.

Although progress has been made in theoretical and computational studies of inertial droplet clustering, clear experimental confirmation is still missing. In particular, computational studies are limited to much lower Reynolds numbers Re_λ than are typically found in atmospheric clouds ($Re_\lambda \sim 10^2$ in direct numerical simulations (DNS) compared to $Re_\lambda \sim 10^5$ in cumulus clouds, where $Re_\lambda \equiv \sigma_u \lambda/\nu$ is the Taylor-Reynolds number with $\lambda = \sigma_u\sqrt{15\nu/\varepsilon}$ the Taylor microscale and σ_u the rms velocity). Thus possible scaling of clustering with Reynolds number remains an open issue (e.g., Jeffery, 2001). Kolmogorov (1962) and Oboukhov (1962) pointed out that in high Reynolds number flows the energy dissipation rate is a highly intermittent quantity.

*Corresponding author.
e-mail: lehmannn@tropos.de
DOI: 10.1111/j.1600-0889.2006.00230.x

Local values of ε, in the following denoted ε_τ, are approximately lognormal distributed (Shaw and Oncley, 2001; Siebert et al., 2006). From eq. (1) it follows that the Stokes number must be a highly intermittent variable as well, even for a constant droplet diameter.

In order to estimate the influence of turbulence on the spatial droplet distribution, simultaneous measurements of the microphysical droplet and turbulence properties at fine spatial resolution are required. Previous observations of droplet clustering in atmospheric clouds made from aircraft platforms (e.g. Baker, 1992; Kostinski and Shaw, 2001; Pinsky and Khain, 2003) are difficult to interpret because only mean turbulence quantities are measured, and because clustering artifacts due to droplet shattering cannot be ruled out. Here we present observational evidence for inertial droplet clustering in turbulent clouds based on measurements of inter-droplet distances and droplet size and local values of the turbulent energy dissipation rate. The measurements were made from a balloon-borne payload at low air speeds to obtain maximum possible spatial resolution, and to preclude droplet shattering. The analyzed cloud field was approximately statistically homogeneous, thereby reducing ambiguities introduced by correcting for large-scale variations in droplet density due to mixing. On the basis of measurements of droplet size and local energy dissipation rate local values of the Stokes number were derived and correlated with the measured droplet spatial distribution.

An overview of the instrumentation utilized in this work is given in Section 2. The methods used for analyzing the spatial distribution of cloud droplets as well as the determination of the local values of the energy dissipation rate are described in Section 3. Finally, observations of the spatial droplet distribution and the relevant turbulence parameters made in cumulus and stratus clouds are shown and discussed.

2. Instrumentation

The measurements were obtained using the Airborne Cloud-Turbulence Observation System (ACTOS), which was suspended from a tethered balloon (Siebert et al., 2003). The ACTOS instrumental payload is equipped with sensors to measure the three-dimensional wind vector, static air temperature, and humidity with a sampling frequency of at least 100 Hz. The wind vector is measured by an ultrasonic anemometer. The measurement of the wind vector refers to a payload-fixed coordinate system and, therefore, has to be corrected for attitude and motion of ACTOS. This is done by means of a navigation unit including a differential Global Positioning System (GPS), an inertial navigation system and a high-resolution barometer. A condensation particle counter measures the number concentration of interstitial aerosol particles in the size range between 12 and 1500 nm. A Particle Volume Monitor (PVM-100A) (Gerber, 1991) measures the liquid water content (LWC). Cloud droplet number density N_D and droplet size distribution are obtained from measurements with the M-Fast-FSSP, which records sizes and arrival times of individual droplets (Schmidt et al., 2004). The ACTOS turbulence sensors are mounted on a 1.5-m-long outrigger; two tail units keep ACTOS in the mean wind direction. In order to minimize flow distortions, ACTOS was fixed 20 m beneath the tethered balloon.

3. Methods

3.1. Local droplet clustering

In order to study the influence of the turbulence of the velocity field on the spatial distribution of droplets, the droplet counting statistics obtained by the M-Fast-FSSP are analyzed and departures from a perfectly random distribution (Poisson process) are quantified using the pair correlation function $\eta(l)$. Specifically, $\eta(l)$ is obtained by first converting the time-series of droplet arrival times measured by the M-Fast-FSSP into a series of droplet distances via the mean droplet velocity (Taylor's hypothesis). This time-series is subdivided into spatial segments δl small enough as to contain only 1 or 0 droplets. In our study, $\delta l = 8 \times 10^{-5}$ m was used. Then $\eta(l)$ is defined as (Shaw et al., 2002):

$$\eta(l) \equiv \frac{\langle N(0) \cdot N(l) \rangle}{\langle N \rangle^2} - 1, \tag{2}$$

where $N(0)$ and $N(l)$ are the number of droplets in bins of width δl separated by distance l. Then $\langle N(0) \cdot N(l) \rangle$ gives the mean number of droplet pairs separated by distance $l \pm \delta l$, and $\langle N \rangle$ is the mean number of droplets for the analyzed time-series. For droplet counts that follow the Poisson process, $\eta(l) \equiv 0$ for all length scales l. If clustering occurs at a length scale l, $\eta(l)$ increases for this scale. At scales below the spatial resolution of the M-Fast-FSSP ($\sim$200 μm), $\eta(l)$ drops to -1. Figure 1 shows a raw and smoothed curve of $\eta(l)$ for a clustered droplet population recorded on May 22, 2003. In order to minimize the noise of $\eta(l)$ caused by the counting statistics, a scale dependent smoothing is applied (black line) to the raw curves of $\eta(l)$ (grey line). The scale dependent smoothing averages out the variability of $\eta(l)$ at large scales, but retains the possible clustering signal at small scales.

For an estimate of the pair correlation function, the counting process has to be statistically stationary, that is, the mean and variance of the number of counts are assumed to be constant over the analyzed time interval. On the other hand, the more droplets used for calculating $\eta(l)$, the more statistically significant the results will be. Thus, for the calculation of $\eta(l)$, a compromise between statistical homogeneity and counting statistics has to be found. Large-scale inhomogeneities of the droplet concentration during the analyzed intervals due to mixing or entrainment cause $\eta(l)$ to be offset for all scales less than that of the scale of the inhomogeneity. If that was the case, the time-series of inter droplet distances was subdivided into smaller intervals, for which the droplet concentration could be considered homogeneous, and

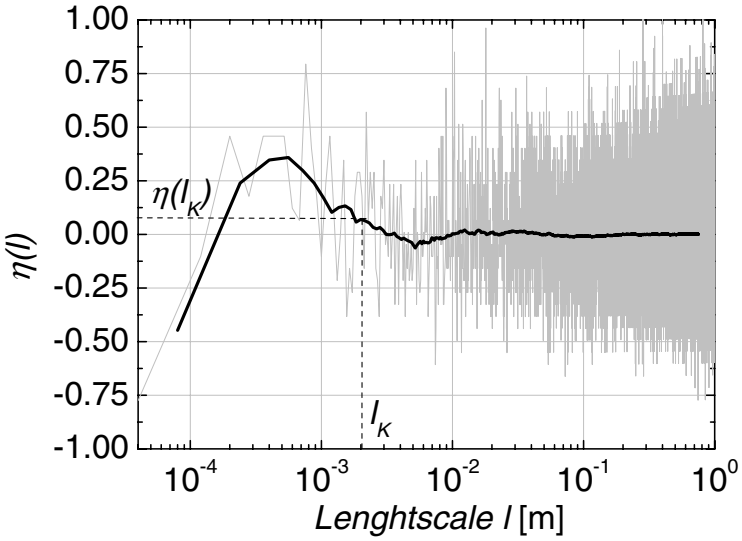

Fig. 1. Raw (grey line) and smoothed (black line) pair correlation function for a clustered droplet population.

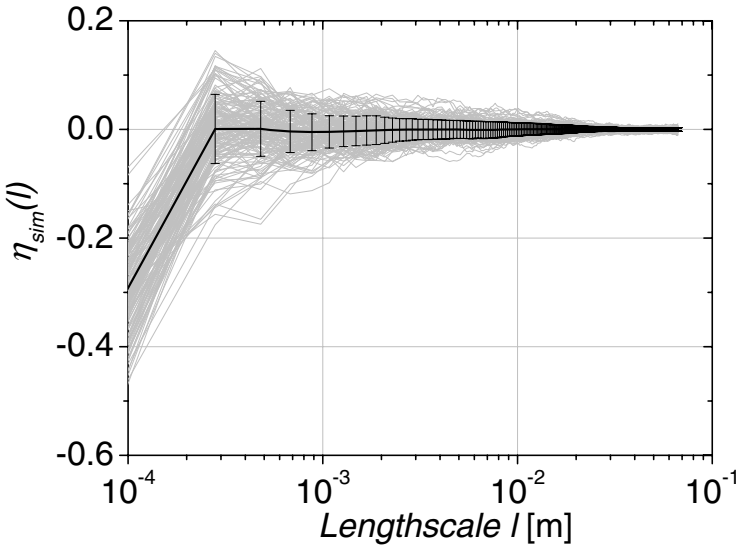

Fig. 2. 100 realizations of the pair correlation function (grey line) for a simulated random droplet distribution. The mean (black line) along with the standard deviation (vertical bars) as well as the maximum and minimum (dotted lines) of the ensemble are displayed.

$\eta(l)$ was calculated as an average of the pair correlation function of each of those sub intervals. If less than 1500 droplets were available for calculating $\eta(l)$, the data were excluded from analysis.

Because clustering of droplets is associated with vortices with size on the order of the Kolmogorov microscale $l_K = (\nu^3/\varepsilon)^{1/4}$, the pair correlation function at this scale $\eta(l_K)$ was used as a measure of the local droplet clustering that allows for physically meaningful comparison of results from different turbulent flows.

For an estimate of the uncertainty of $\eta(l)$, a randomly distributed droplet population was generated with the same droplet number density as the analyzed atmospheric clouds. Out of this volume with randomly distributed droplets, the volume swept out by the M-Fast-FSSP was simulated, and pair correlation functions $\eta_{\mathrm{sim}}(l)$ for subsequent independent intervals with a comparable length L as analyzed for the atmospheric clouds were calculated. Figure 2 shows 100 realizations of $\eta_{\mathrm{sim}}(l)$ (grey lines) for a droplet number density N_D of 750 cm^{-3}, which, with the M-Fast-FSSP's sampling cross section of 0.15 mm^2, gives a counted rate of $\lambda = 113$ m^{-1}. Clearly the uncertainty $\sigma_{\eta_{\mathrm{sim}}}$ (vertical bars) increases with decreasing lengthscale l, which could be falsely interpreted as clustering. The increasing variability of $\eta_{\mathrm{sim}}(l)$ with decreasing lengthscale is due to the scale dependent smoothing, where fewer points are used for averaging at small scales to retain the possible clustering signature (cf. Fig. 1). The standard deviation $\sigma_{\eta_{\mathrm{sim}}(l_K)}$ of 100 realizations of η_{sim} at the Kolmogorov microscale l_K is used as a limit that separates values of $\eta(l)$ that are due to the sampling statistics from those that indeed indicate clustering. Assuming that the 100 realizations of $\eta_{\mathrm{sim}}(l)$ are normally distributed, the relative error of $\sigma_{\eta_{\mathrm{sim}}(l_K)}$ is 7%.

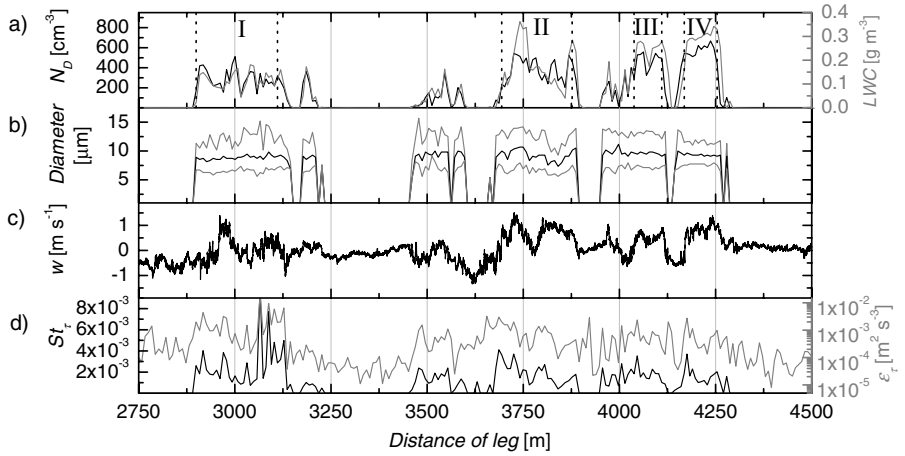

Fig. 3. Record of droplet number concentration and LWC (grey line) (a), median droplet diameter (black line) together with the 5th and 95th percentile of the droplet size distribution (grey lines) (b), vertical velocity (c), local Stokes number (black line) and local energy dissipation rate (grey line) for May 19, 2003.

3.2. Local energy dissipation rates

Determination of the droplet Stokes number requires the turbulent kinetic energy dissipation rate to be known (cf. eq. 1). The small-scale structure of the turbulence can be investigated by means of what we will refer to as the 'local' energy dissipation rates ε_τ, where the index τ indicates the averaging time over which the parameter is estimated ($\tau = 2$ and 5 s in our study) (Muschinski et al., 2004; Siebert et al., 2006).

In this work, ε_τ is estimated from the 2nd-order structure function $D_u^\tau(t') = \langle (u(t+t') - u(t))^2 \rangle_\tau$ of the detrended longitudinal wind velocity component u (Frisch, 1995, sec. 6.3.1), which, in the inertial subrange, is given by:

$$D_u^\tau(t') = 2\,\varepsilon_\tau^{2/3}\,(t' \langle u \rangle_\tau)^{2/3}, \tag{3}$$

and, therefore,

$$\varepsilon_\tau = (0.5\,D_u^\tau(t'))^{3/2} / (t' \langle u \rangle_\tau) \tag{4}$$

with the time lag t' and $\langle u \rangle_\tau$ the mean of u during τ. By using ε_τ in eq. (1) it is possible to estimate local Stokes numbers St_τ.

4. Measurements

The data were recorded during the Baltex Bridge Campaign (BBC2) (Crewell et al., 2004) in Cabauw, The Netherlands. Three case studies will be presented, two horizontal passages through Cumulus humilis (Cu hum) clouds and a vertical profile through a stratus cloud. For all of these clouds, the level of turbulence is relatively low, with $\langle \varepsilon_\tau \rangle$ below 10^{-2} m^2 s^{-3}, and $\langle St_\tau \rangle \lesssim 10^{-2}$.

4.1. Observed cumulus clouds

Figure 3 shows a record of droplet number density N_D (a), liquid water content LWC (a, grey line, right scale), the median droplet diameter $\langle d \rangle$ together with the 5th and 95th percentiles of the droplet size distribution (b), the vertical wind velocity w (c) and St_τ (d) as well as ε_τ (d, grey line, right scale) for a passage through Cu hum clouds on May 19, 2003. Varying values of N_D between 200 and 700 cm^{-3} indicate partly diluted, aged clouds. Weak updrafts and downdrafts with maximal values of w of ± 1.5 m s^{-1} exist, but are not necessarily correlated with ε_τ. Lowest values of $\varepsilon_\tau = 10^{-5}$ m^2 s^{-1} are located in cloud free regions, whereas values of $\sim 10^{-2}$ m^2 s^{-1} can be found inside the clouds. With a mean droplet diameter of 9 μm, maximum values of $St_\tau = 10^{-2}$ are calculated. For each of the four marked cloud penetrations, $\eta(l)$ was calculated (Fig. 4). Additionally, the mean and $\sigma_{\eta_{\mathrm{sim}}(l)}$ of 100 realizations of $\eta_{\mathrm{sim}}(l)$ for a randomly distributed droplet population with the same λ and L as the analyzed cloud passages are shown. Clearly, the reliabilty of $\eta(l)$ increases with

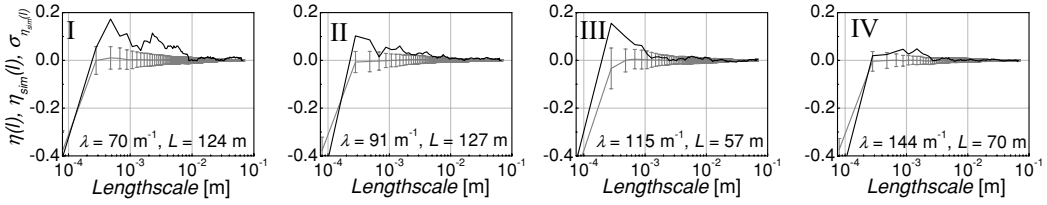

Fig. 4. Pair correlation functions (thick black line) for each of the marked cloud regions in Fig. 3, as well as the mean (grey line) and the standard deviation (vertical bars) for a simulated random droplet distribution.

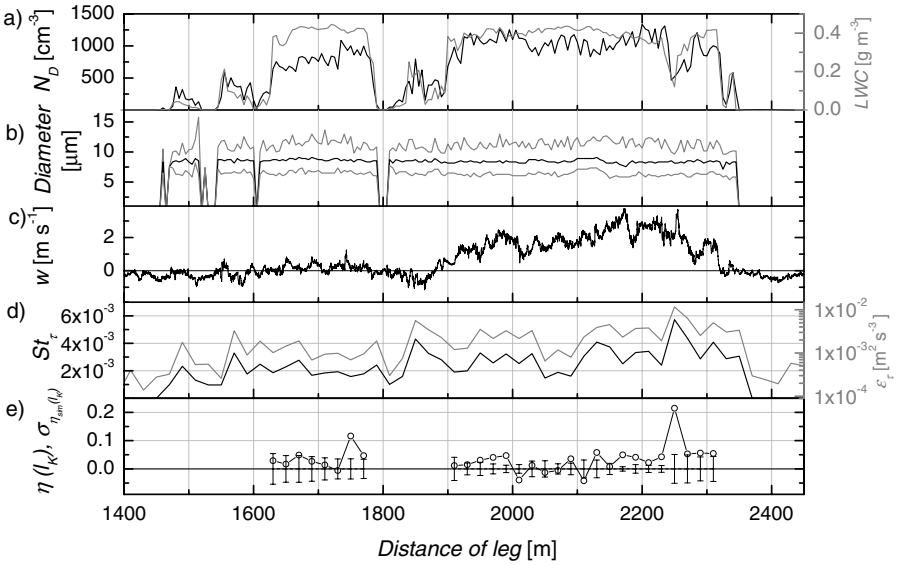

Fig. 5. Record of droplet number concentration and LWC (grey line) (a), median droplet diameter (black line) together with the 5th and 95th percentile of the droplet size distribution (grey lines) (b), vertical velocity (c), local Stokes number (black line) and local energy dissipation rate (grey line) as well as the pair correlation function at the Kolmogorov microscale (open circles) and the standard deviation of the synthetic pair correlation functions for a random droplet population (vertical bars) for May 21, 2003.

increasing λ and increasing L. For the first three cloud passages, $\eta(l)$ exceeds the uncertainty of $\eta(l)_{\rm sim}$, thus clearly indicating droplet clustering.

A similar analysis was applied to Cu hum clouds measured on May 21, 2003. During that day, unusually high values of N_D up to 1400 cm^{-3} were encountered, yielding a high λ up to 210 m^{-1} and allowing for calculation of $\eta(l)$ with a temporal resolution of 2 s, equivalent to ∼ 15 m. Figure 5 shows N_D and LWC (a), $\langle d\rangle$ together with the 5th and 95th percentiles of the droplet size distribution (b), w (c) and St_τ (d) as well as ε_τ. The local energy dissipation rate ε_τ varies between 10^{-4} m^2 s^{-1} in cloud free regions and 10^{-2} m^2 s^{-1} in the most turbulent part of the clouds. This yields, for the small $\langle d\rangle$ of 8.5 μm encountered, $St_\tau < 6 \times 10^{-3}$. On panel e), $\eta(l_K)$ is displayed, as well as $\sigma_{\eta_{\rm sim}(l_K)}$ for a random droplet distribution with the local λ and $L = 15$ m. Most $\eta(l_K)$ are positive and barely exceed the uncertainty of $\eta_{\rm sim}(l_K)$. Between 2130 and 2310 m of the leg $\eta(l_K)$ clearly indicates droplet clustering. This is also a region where St_τ is at its largest values. Especially at about 2250 m of the leg, the maximum of $\eta(l_K)$ coincides with a maximum of St_τ and ε_τ. However, this regions is marked by a sharp drop in number density, which partly decreases the confidence in $\eta(l_K)$ by reducing λ and the homogeneity of the sample.

4.2. *Observed stratus clouds*

Between 8:55 and 10:10 UTC on May 22, 2003, ACTOS measured vertical profiles through a low stratus cloud ($Re_\lambda \sim 10^5$). Figure 6 shows the profile of LWC (a), N_D (b), $\langle d\rangle$ together with the 5th and 95th percentiles of the drop size distribution (c), ε_τ (d), aerosol particle number concentration N_P (e), wind direction dd and wind speed U (f) taken during a descent. For all parameters, 5 s was used as averaging time, yielding a vertical resolution of 2.5 m and a horizontal resolution of 40 m. From the profiles of LWC, N_D and N_P it can be seen that the stratus cloud consists of two layers. LWC has a distinct minimum at about 620 m above ground level (AGL). For N_D and N_P, the difference between the two cloud layers is even more distinct. In the lower cloud layer, both reveal large fluctuations, and remain at nearly constant values in the upper cloud layer. Interestingly, the separation of the two cloud layers is not apparent in $\langle d\rangle$. Generally, $\langle d\rangle$ increases linearly with height and the 5th and 95th percentiles of the droplet size distribution indicate a broadening of the droplet size distribution with height. The detachment of the two cloud layers is caused by the top of the planetary boundary layer (PBL) at about 500–600 m. This becomes obvious in the profile of ε_τ (calculated from eq. (3) with $\tau = 5$ s), which shows a decrease of ε_τ with height to about 600 m, whereas above this height, ε_τ remains nearly constant. Similarly, the profiles of dd and U reveal large gradients in the lower cloud layer, confirming that the dynamics of the flow changes rapidly in the PBL, whereas both dd and U remain quite constant in the upper part of the analyzed profile. In Fig. 7, $\eta(l_K)$ is displayed as a function of height. Additionaly $\sigma_{\eta_{\rm sim}(l_K)}$ is shown. In general, the clustering of droplets becomes more intense with height until a level of ∼950 m is reached. Nearly at all levels $\eta(l_K)$ reaches values that cannot be explained by the uncertainty of $\eta(l_K)$ for a random droplet distribution. In the gap of the profile of $\eta(l_K)$, not enough droplets (<1500 or $\lambda < 37$ m^{-1}) were available for a reasonable calculation of $\eta(l_K)$.

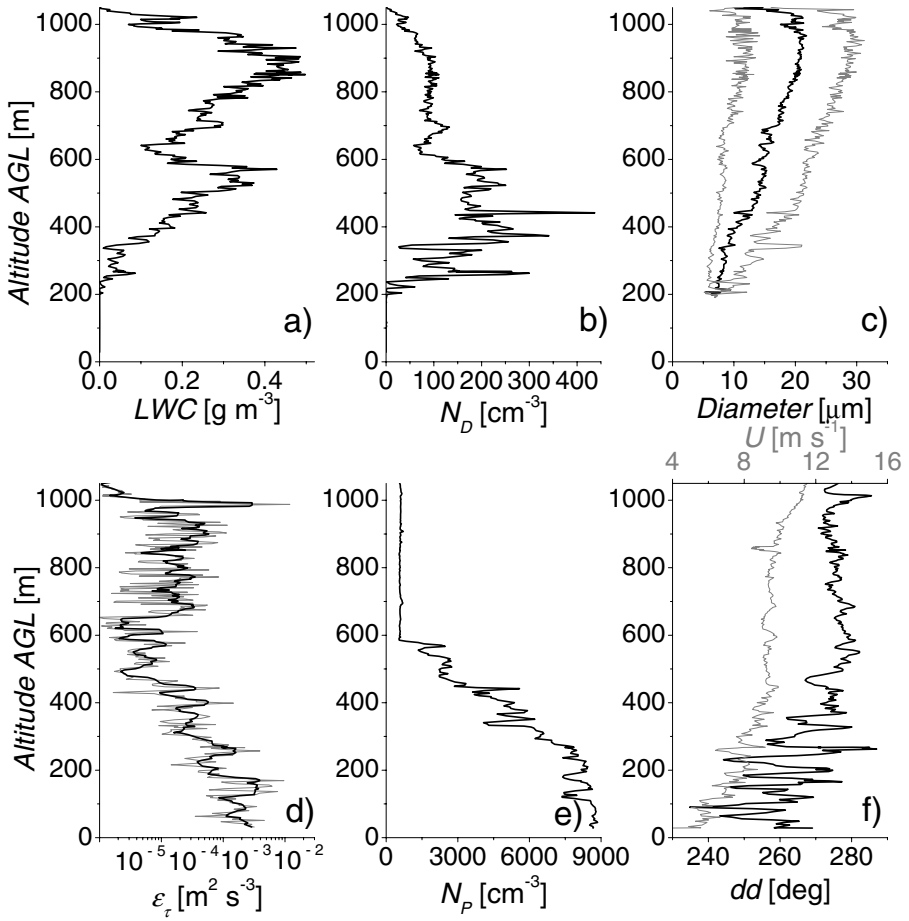

Fig. 6. Profile of LWC (a), droplet number concentration (b), median droplet diameter (black line) together with the 5 and 95 percentile of the droplet size distribution (grey lines) (c), raw (grey line) and smoothed (black line) local energy dissipation rate (d), aerosol particle number concentration (e) and wind direction (black line) and speed (grey line) (f) for May 22, 2003.

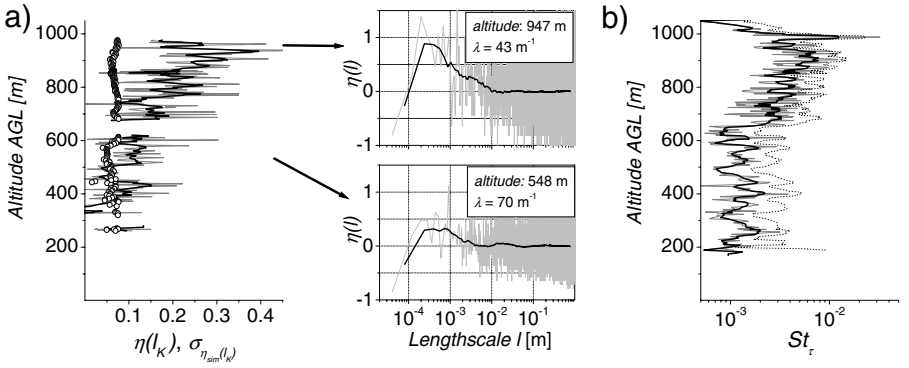

Fig. 7. (a) Profile of raw (grey line) and smoothed (black line) $\eta(l_K)$. The circles indicate the uncertainty derived for a randomly distributed droplet population with the same λ and L. Right to the profile, two exemplary raw and smoothed curves of $\eta(l)$ are shown. (b) Profile of raw (grey line) and smoothed (black line) St_τ, as well as St_τ for the largest droplets of the size distribution (dashed line).

Using ε_τ and the median diameter of the droplet size distribution averaged over τ, local Stokes numbers (St_τ) were calculated from eq. (1). The profile of St_τ is shown in Fig. 7b). Also, the profile of the Stokes number corresponding to the largest droplets of the size distribution is shown (calculated using the 95th percentile of the droplet size distribution). Although exhibiting some structure, St_τ is approximately constant in the PBL, and increases in the upper cloud to a level of about 900 m, where it starts to

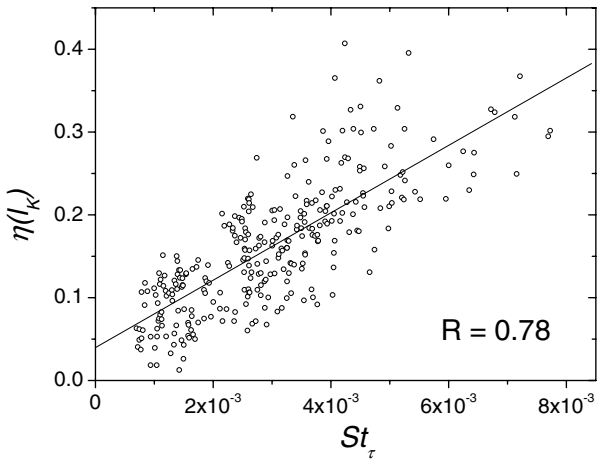

Fig. 8. Correlation plot of St_τ and $\eta(l_K)$.

decrease again. The result of a linear regression between the 5 point running averages of $\eta(l_K)$ and St_τ is displayed in Fig. 8. Data from two ascents before and after the descent shown in Figs. 6 and 7 are included as well, thus altogether 297 pair correlation functions remained for analysis. The correlation coefficient for a linear dependence of $\eta(l_K)$ on St_τ is $R = 0.78$.

5. Discussion and conclusion

The primary finding of this study is the indication of droplet clustering even in weakly turbulent clouds. For three analyzed cases, two horizontal passages through cumulus clouds and vertical profiles through a stratus cloud, we found regions where droplets are clustered at sub-cm scales. For cumulus clouds, these regions are localized in space, coexisting with regions where no indication for clustering was found. For vertical profiles through a stratus cloud, for which St_τ slowly increased with height, a correlation of $\eta(l_K)$ and St_τ was found, providing evidence that cloud droplets cluster due to their finite inertia, even in weakly turbulent clouds. While a correlation between $\eta(l_K)$ and St_τ is expected theoretically (even for $St \ll 1$; see for example Falkovich et al., 2002), the magnitude of $\eta(l_K)$ for such small St is surprising. We note, however, that it is not inconsistent with the previous results of Uhlig et al. (1998), who measured clustering in holograms from stratus clouds, and Pinsky and Khain (2003), who found small-scale drop concentration fluctuations in cumulus clouds for $St < 0.01$. However, we were only partly able to obtain such a correlation of $\eta(l_K)$ and St_τ for cumulus clouds. Due to the intermittency of turbulence at high Reynolds numbers, regions of high ε_τ are localized in space, and, in order to obtain a correlation with $\eta(l_K)$, a high spatial resolution of $\eta(l_K)$ is required. Unfortunately, this can only be supplied for high droplet number densities, otherwise the uncertainty of $\eta(l_K)$ does not allow a meaningful interpretation. Another point that needs consideration is caused by the one-dimensional sampling of droplets with the M-Fast FSSP, causing the calculated one-dimensional $\eta(l)$ to be attenuated at scales below the characteristic lengthscale of the instrument (Holtzer and Collins, 2002), an effect that is more pronounced in turbulent clouds with small values of l_K (see Appendix A for further details).

In the past the turbulence has either not been measured or only measured at low spatial resolution, so the local Stokes numbers could not be determined with confidence. Our measurements from ACTOS eliminate this uncertainty and therefore improve our confidence in the results. The most significant challenge in all field studies of clouds is distinguishing clustering due to droplet inertia from clustering due to entrainment and mixing. We have accomplished this through the averaging method described previously. Furthermore, by comparing the pair correlation functions evaluated at a scale in the viscous subrange, where mixing plays only a minor role, we avoid any significant influence of mixing on the results.

Another criticism of previous, aircraft-based measurements has been the possibility that droplet clustering is caused by breakup of droplets impacting on the housing of the droplet sizing instrument. For the balloon-borne measurements at the low true air speeds analyzed in this paper, breakup of impacting droplets is unlikely. The modified Weber number, given by the ratio of the particle kinetic energy to its surface energy

$$We = \frac{\frac{1}{2}\, m\, u_{\mathrm{imp}}^2}{\sigma A} \lesssim 4, \tag{5}$$

for the largest droplets observed and thus well below the critical value of 7–10 for droplet breakup (Hallett and Isaac, 2002). In eq. (5), m and A are the mass and area of the impacting droplet, σ is the surface tension of water and u_{imp} is the impact velocity. It is therefore concluded that the local droplet clustering found in this study is not an artifact caused by droplet breakup on the instrument housing.

As mentioned before, another benefit of the balloon-borne ACTOS is the ability to obtain high resolution turbulence measurements, and, as a result, to derive local energy dissipation rates. Using this approach we have found $\eta(l_k)$ to correlate with with local turbulence properties. This yields an important result: because ε_τ is a highly intermittent quantity (Siebert et al., 2006), the correlation between local turbulence parameters and clustering has implications for the production of large, 'lucky' drops that may serve to initiate the growth of drizzle via droplet coalescence (Kostinski and Shaw, 2005). Intermittent pockets of cloud that are vigorously turbulent would be envisioned to serve as zones of enhanced droplet coalescence. Subsequent mixing of large droplets produced in these zones could lead to accelerated rain formation. Interestingly, because energy dissipation rates (and therefore droplet Stokes numbers) tend to peak in regions where entrainment is strongest, there apparently will be a competition between dilution due to entrainment, and enhancement of collision rates due to inertial clustering. The relative roles of the two competing effects remains an open problem.

Future work will be devoted to make a detailed comparison between measurements and computational/theoretical results, especially to understand the possible dependence of inertial droplet clustering on Reynolds number. We may safely conclude, however, that the correlation between Stokes number and pair correlation function observed in this study provides compelling evidence that inertial clustering occurs even for relatively small droplets in weakly turbulent clouds. In turn, any clustering, regardless of its origin, will contribute to an enhanced collision rate compared to that predicted from mean droplet number densities (Sundaram and Collins, 1997), as are typically used in cloud models.

6. Acknowledgments

We thank the German Bundeswehr and G. Sanftleben and his coworkers from the Bundeswehr Technical Centre for Ships and Naval Weapons for kindly providing and operating the tethered balloon. We thank the Dutch weather service (KNMI) and enviscope GmbH for their support during the BBC2 campaign. Also, the authors would like to thank Sebastian Schmidt for his efforts with the M-Fast-FSSP. Part of this work was funded by the Deutsche Forschungsgemeinschaft (WE 1900/7-1/2). R. Shaw acknowledges support from the U.S. National Science Foundation (grant ATM-0320953).

7. Appendix A

The M-Fast FSSP measures the time that passes between droplets that pass the laser beam in a long narrow tube with an ellipsoidal cross section. Figure 9 shows a sketch of the M-Fast FSSP's sampling volume geometry. The sensitive cross section of the M-Fast FSSP has a length of ~ 6 mm and a width of $\sim 200\,\mu$m,

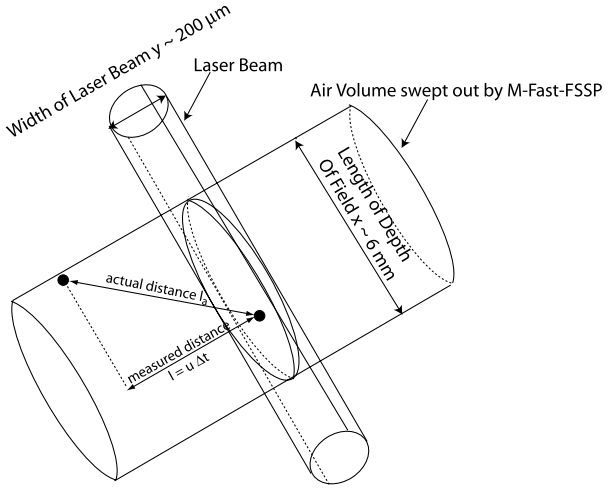

Fig. 9. Sketch of the M-Fast FSSP's sensitive cross section and the swept air volume.

thus the actual distance l_a between droplets passing the laser beam is given by $l_a = (l^2 + x^2 + z^2)^{1/2}$, with l determined by the interarrival time Δt and the longitudinal velocity u, and $0 < x < 6$ mm and $0 < z < 200\,\mu$m. Thus $\eta(l)$ contains information from scales l to l_a. This causes the one-dimensional $\eta(l)$ to be lower than the actual three dimensional pair correlation function. Following Holtzer and Collins (2002) this attenuation becomes effective at lengthscales close to the characteristic lengthscale l_c of the instrument. To further complicate matters, the geometry of the M-Fast FSSP's sampling volume is not only asymmetric, but the size of the sampling volume depends on droplet size (Schmidt et al., 2004), thus an estimation of the characteristic lengthscale is nearly impossible. However, it is clear that when the Kolmogorov microscale, the scale at which we evaluate clustering in this study, is larger than l_c, $\eta(l)$ will deviate less from the three-dimensional pair correlation function than if $l_K < l_c$. For the low energy dissipation rates measured in the Stratus cloud, $l_K > l_c$ and the attenuation of $\eta(l)$ is not significant, however, for more turbulent cumulus cloud, $l_K \lesssim l_c$, so $\eta(l)$ is possibly attenuated. It follows that it is easier to detect clustering in weakly turbulent clouds, where the Kolmogorov microscale is larger than in more turbulent cumulus clouds. Moreover, as in turbulent clouds ε_τ changes from 10^{-4} to $10^{-2}\,\mathrm{m^2\,s^{-3}}$ in a couple of meters, l_K decreases from 2.5 mm to 760 μm, providing constantly changing degree of attenuation of $\eta(l)$. This problem can partly be overcome by only analyzing droplets that pass the laser beam at its center, thus reducing l_c. This was done for the cumulus cloud analyzed in this paper. On the other hand, this reduces the number of available droplets to calculate $\eta(l)$ and thus increases the uncertainty due to statistical noise.

References

Baker, B. 1992. Turbulent entrainment and mixing in clouds: A new observational approach. *J. Atmos. Sci.* **49**, 387–404.

Crewell, S., Simmer, C., Bloemink, H., Feijt, A., Garcia, S. and coauthors. 2004. The BALTEX Bridge Campaign: An integrated approach for a better understanding of clouds. *Bull. Am. Meteor. Soc.* **85**, 1565–1584.

Falkovich, G., Fouxon, A. and Stepanov, M. G. 2002. Acceleration of rain initiation by cloud turbulence. *Nature* **419**, 151–154.

Franklin, C. N., Vaillancourt, P. A., Yau, M. K. and Bartello, P. 2005. Collision rates of cloud droplets in turbulent flow. *J. Atmos. Sci.* **62**, 2451–2466.

Frisch, U. 1995. *Turbulence - The Legacy of A. N. Kolmogorov*. Cambridge University Press, Cambridge, England, 296 pp.

Gerber, H. 1991. Direct measurement of suspended particulate volume concentration and far-infrared extinction coefficient with a laser-diffraction instrument. *Appl. Opt.* **30**, 4824–4831.

Hallett, J. and Isaac, G. A. 2002. Aircraft icing in glaciated and mixed phase clouds. In *Proceedings 40th AIAA Aerospace Science Meeting and Exhibit.*, Reno, Nevada, USA. 14–17 January 2002.

Holtzer, G. L. and Collins, L. R. 2002. Relationship between the intrinsic radial distribution function for an isotropic field of particles and lower-dimensional measurements. *J. Fluid Mech.* **459**, 93–102.

Jeffery, C. A. 2001. Investigating the small-scale structure of clouds using the δ-correlated closure: effect of particle inertia, condensation/evaporation and intermittency. *Atmos. Res.* **59–60**, 199–215.

Kolmogorov, A. N. 1962. A refinement of previous hyotheses concerning the local structure of turbulence in a viscous incompressible fluid at high Reynolds number. *J. Fluid Mech.* **13**, 82–85.

Kostinski, A. B. and Shaw, R. A. 2001. Scale-dependent droplet clustering in turbulent clouds. *J. Fluid Mech.* **434**, 398–398.

Kostinski, A. B. and Shaw, R. A. 2005. Fluctuations and luck in droplet growth by coalescence. *Bull. Am. Meteor. Soc.* **86**, 235–244.

Maxey, M. R. 1987. The gravitational settling of aerosol particles an homogeneous turbulence and random flow fields. *J. Fluid Mech.* **174**, 441–465.

Muschinski, A., Frehlich, R. G. and Balsley, B. B. 2004. Small-scale and large-scale intermittency in the nocturnal boundary layer and the residual layer. *J. Fluid Mech.* **515**, 319–351.

Oboukhov, A. M. 1962. Some specific features of atmospheric turbulence. *J. Fluid Mech.* **13**, 77–81.

Pinsky, M. and Khain, A. 2003. Fine structure of cloud droplet concentration as seen from the Fast-FSSP measurements. Part II: Results of in situ observations. *J. Appl. Meteor.* **42**, 65–73.

Pruppacher, H. and Klett, J. 1997. *Microphysics of Clouds and Precipitation*. Kluwer Academic Publishers, Dordrecht, The Netherlands, 953 pp.

Saffman, P. G. and Turner, J. S. 1956. On the collision of drops in turbulent clouds. *J. Fluid Mech.* **1**, 16–30.

Schmidt, S., Lehmann, K. and Wendisch, M. 2004. Minimizing instrumental broadening of the drop size distribution with the M-Fast-FSSP. *J. Atmos. Oceanic Technol.* **21**, 1855–1867.

Shaw, R. A. 2003. Particle-turbulence interactions in atmospheric clouds. *Annu. Rev. Fluid Mech.* **35**, 183–227.

Shaw, R. A. and Oncley, S. P. 2001. Acceleration intermittency and enhanced collision kernels in turbulent clouds. *Atmos. Res.* **59**, 77–87.

Shaw, R. A., Kostinski, A. B. and Larsen, M. L. 2002. Towards quantifying droplet clustering in clouds. *Q. J. R. Meteorol. Soc.* **128**, 1043–1057.

Siebert, H., Wendisch, M., Conrath, T., Teichmann, U. and Heintzenberg, J. 2003. A new tethered balloon-borne payload for fine-scale observations in the cloudy boundary layer. *Boundary-Layer Meteorol.* **106**, 461–482.

Siebert, H., Lehmann, K. and Wendisch, M. 2006. Observations of small scale turbulence and energy dissipation rates in the cloudy boundary layer. *J. Atmos. Sci.* **63**, 1451–1466.

Sundaram, S. and Collins, R. 1997. Collision statistics in an isotropic particle-laden turbulent suspension. Part I: Direct numerical simulation. *J. Fluid Mech.* **335**, 75–109.

Tennekes, H. and Lumley, J. L. 1972. *A First Course in Turbulence*. The MIT Press, Cambridge, MA, USA, 300 pp.

Uhlig, E.-M., Borrmann, S. and Jaenicke, R. 1998. Holographic in-situ measurements of the spatial droplet distribution in stratiform clouds. *Tellus* **50B**, 377–387.

Wang, L.-P. and Maxey, M. R. 1993. Settling velocity and concentration distribtuion of heavy particles in homogeneous isotropic turbulence. *J. Fluid Mech.* **256**, 27–68.